JURNAL
BIOS LOGOS
Accredited by Ministry of Research, Technology and Higher Education No. 105/E/KPT/2022

Vol. 16 (No.1), Maret 2026, 118-142
DOI: https://doi.org/10.35799/jbl.v16i1.67558
E-ISSN: 2656-3282
P-ISSN: 2088-9569

Integrative In Silico Discovery of *Ficus minahassae* Fruit-Derived Compounds as Selective Inhibitors of EGFR L858R in Lung Cancer Therapy

Rendy Victor Worotikan[1,2], Feky Recky Mantiri[1], Trina Ekawati Tallei[1,2,3]*
[1]Department of Biology, Faculty of Mathematics and Natural Sciences, Sam Ratulangi University. Kampus Bahu Street, Manado 95115, North Sulawesi, Indonesia, Telp./Fax. (0431) 864386/ 85371.
[2]Molecular Biology Laboratory, Sam Ratulangi University, Manado 95115, North Sulawesi, Indonesia
[3]Department of Biology, Faculty of Medicine, Sam Ratulangi University, Manado 95115, North Sulawesi, Indonesia
*email correspondece: trina_tallei@unsrat.ac.id

(Article History: Received-May 4th, 2026; Revised-July 31st, 2026; Accepted- July 31st, 2026)

Abstract. Lung cancer remains the leading cause of cancer-related mortality worldwide, with Epidermal Growth Factor Receptor (EGFR) mutations, particularly L858R, driving the progression and drug resistance of non-small cell lung cancer (NSCLC). *Ficus minahassae* (Langusei), an endemic species of North Sulawesi, contains diverse bioactive metabolites whose anticancer potential has not been explored. This study evaluated the potential of Langusei fruit metabolites as EGFR L858R inhibitors through an integrative in silico approach. Metabolites were identified via gas chromatography–mass spectrometry (GC–MS) and liquid chromatography–high-resolution mass spectrometry (LC–HRMS). Target prediction was conducted using SwissTargetPrediction (probability > 0.5) and the Similarity Ensemble Approach (SEA) (MaxTC > 0.5), while NSCLC-related targets were retrieved from OMIM, GeneCards, Genpia2, DisGeNET, and cBioPortal. Network pharmacology and CytoHubba topology analyses were used to identify hub proteins, followed by ADMET profiling and molecular docking to assess binding affinity toward EGFR wild type and L858R mutant. A total of 170 metabolites were identified, dominated by fatty acyls, prenol lipids, and steroid derivatives. Integration of target prediction and disease databases revealed 355 overlapping proteins, among which seven hub proteins, including EGFR, STAT3, EP300, HSP90AA1, JUN, HIF1A, and ESR1, were identified as key regulators of oncogenic pathways. Molecular docking demonstrated that (Z)-1-(1,3-benzodioxol-5-yl)-3-methoxy-3-(2,4,6-trimethoxyphenyl)prop-2-en-1-one exhibited strong binding affinities to both EGFR wild type and L858R mutant and possessed a favorable ADMET profile comparable to Gefitinib and Osimertinib. These findings highlight Langusei fruit as a promising natural source of safe, multi-target EGFR inhibitors with potential therapeutic relevance for NSCLC. Further in vitro and in vivo validation is warranted to confirm efficacy and selectivity.
Key words: *Ficus minahassae*; Langusei fruit; non-small cell lung cancer; EGFR L858R mutation; in silico analysis; natural inhibitors

INTRODUCTION

Lung cancer remains the leading cause of cancer-related mortality worldwide, accounting for approximately 1.8 million deaths in 2022, or about 18–19% of all cancer deaths. In non-small cell lung cancer (NSCLC), mutations in the Epidermal Growth Factor Receptor (EGFR) are major drivers of disease progression and therapeutic response. However, resistance to even the latest generations of EGFR inhibitors remain common, underscoring the urgent need for novel therapeutic candidates and broader targeting strategies (Bray et al., 2024; Zhou et al., 2024). To address these therapeutic challenges, systems-based approaches such as metabolomics have emerged as powerful tools to identify novel bioactive compounds and elucidate their molecular targets in cancer.

The metabolomics approach enables comprehensive mapping of both endogenous and exogenous metabolites and is increasingly adopted across the drug discovery pipeline—from elucidating disease mechanisms and identifying or validating molecular targets to dereplication, lead compound prioritization, and prediction of drug responses. This method has proven highly effective when integrated with in silico techniques such as network pharmacology and molecular docking, allowing resource-efficient hypothesis screening prior to experimental validation (Wishart, 2026; Pang & Hu, 2023). Such integrative strategies

offer promising opportunities to explore bioactive compounds from endemic biological sources that may target key molecular nodes involved in cancer.

Ficus minahassae (Langusei), an endemic plant of North Sulawesi, remains underexplored, although preliminary findings suggest its potential for systematic metabolomic investigation. To date, no study has mapped its metabolites and linked them in silico to NSCLC-related molecular targets, particularly EGFR L858R and angiogenesis-related pathways. The Epidermal Growth Factor Receptor occupies a central role in NSCLC pathogenesis; the L858R mutation within its tyrosine kinase domain drives constitutive activation, promoting proliferation, survival, and resistance to apoptosis and tyrosine kinase inhibitors (Delaney et al., 2015; La Monica, 2022; Fu et al., 2022).

At the molecular level, the Epidermal Growth Factor Receptor (EGFR) occupies a central position in the pathogenesis of non-small cell lung cancer (NSCLC). The L858R mutation within the tyrosine kinase domain of EGFR is among the most prevalent genetic alterations and serves as a key determinant of constitutive receptor activation, driving cancer cell proliferation, survival, and resistance to apoptosis. Hyperactivation of the EGFR signaling pathway not only initiates tumor growth but also contributes to immune evasion and resistance to first-generation tyrosine kinase inhibitor (TKI)–based therapies. Therefore, the identification of alternative inhibitors capable of targeting EGFR, particularly the L858R mutant variant, remains a critical focus in the advancement of precision therapy for NSCLC (Delaney et al., 2015; La Monica, 2022; Fu et al., 2022).

This study aimed to integrate metabolomic profiling of *Ficus minahassae* extract with network pharmacology and molecular docking analyses to generate a comprehensive mapping of its chemical landscape, while simultaneously predicting and prioritizing therapeutic targets relevant to NSCLC, including those associated with EGFR L858R mutation and angiogenesis-related pathways. Through this integrative approach, a robust scientific basis was expected to be established for developing natural inhibitor candidates derived from Indonesia's biological resources that specifically target EGFR.

METHODS

Study Site and Sampling

This study integrated metabolomic profiling of *Ficus minahassae* extract using gas chromatography–mass spectrometry (GC–MS) and liquid chromatography–high-resolution mass spectrometry (LC–HRMS) with network pharmacology and molecular docking analyses. These complementary analytical platforms enabled the comprehensive detection of volatile and semi-polar metabolites, providing a robust chemical profile for identifying therapeutic targets associated with NSCLC, particularly EGFR L858R mutation and angiogenesis pathways. The research was conducted from July 2025 to October 2025, and the sample collection site was Minahasa, North Sulawesi, Indonesia (1°25'48.4" LU 124°52'06.0" BT).

Sample Preparation

Ripe Langusei fruits were air-dried at room temperature under light-protected conditions, ground into powder, and sequentially extracted with ethanol with of 1:10 w/v, for 3 × 24 h with gentle agitation. The filtrates were passed through 0.22 µm filters and evaporated under vacuum at ≤40°C. Metabolite profiling was conducted using GC-MS and LC-HRMS.

GC – MS Analysis

GC–MS analysis was performed using a Thermo Fisher Scientific system (model ISQD1702517_1) operated with Chromeleon software version 7.2.10.24543. Two solvents, n-hexane and ethanol, were used for sample preparation. The analysis employed electron ionization (EI) at 70 eV, with the ion source and transfer line temperatures both set at 280 °C. Separation was achieved on a non-polar capillary column (5% phenyl–methylpolysiloxane, 30 m × 0.25 mm × 0.25 µm). The oven temperature was programmed from 60 °C to 300 °C at 10 °C min^{-1} and held for 10 min, giving a total run time of 39 min. Helium served as the carrier gas at 1.0 mL min^{-1}. One microliter of each sample was injected in split mode (10:1). Mass spectra were acquired in centroid mode over an m/z range of 40–500. Compound identification was based on NIST library matching and retention index comparison, retaining features with a match factor ≥80 and consistent detection across replicates.

LC-HRMS Analysis

Metabolomic profiling was performed using a Thermo Scientific™ Vanquish™ Horizon UHPLC coupled to an Orbitrap™ Exploris 240 HRMS with an OptaMax™ NG heated ESI source. Separation was achieved on an Accucore™ Phenyl Hexyl column (100 × 2.1 mm, 2.6 µm) at 40 °C using a mobile phase of (A) water with 0.1% formic acid and (B) acetonitrile with 0.1% formic acid at 0.3 mL·min^{-1}. The gradient was 5–90% B in 16 min, held for 4 min, and returned to 5% B (total run time 25 min); injection volume was 5 µL. The Orbitrap operated in polarity-switching mode with full MS/dd-MS^2 acquisition (resolution 60,000 FWHM; m/z 70–800; NCE 30, 50, 70). Source parameters were: spray voltage +3500/–2500 V, sheath gas 35 AU, auxiliary gas 7 AU, ion transfer tube 300 °C, vaporizer 320 °C. Metabolites were extracted using both methanol and n-hexane solvents (50 mg per 1 mL), followed by vortexing (1 min), ultrasonication (30 min), centrifugation (1400 × g, 20 °C, 5 min), and filtration through a 0.20 µm nylon membrane. Data processing was conducted in Compound Discoverer 3.3 using mzCloud, ChemSpider, and Mass List databases (ChEBI, KEGG, LIPID MAPS, PubChem, and Natural Products Atlas).

Target Protein Selection

Proteins associated with non-small cell lung cancer (NSCLC) were identified by integrating multiple databases: OMIM for genetic disease genes, GeneCards for gene functions and molecular pathways, Gepia2 for gene–protein interactions, DisGeNET for gene–disease associations, and cBioPortal for patient-derived genetic alterations. Predicted targets of *F. minahassae* metabolites were obtained using SwissTargetPrediction (probability > 0.5) and the Similarity Ensemble Approach (SEA) (MaxTC > 0.5), retaining only medium- to high-confidence targets to minimize false positives and ensure biological and clinical relevance to NSCLC.

Network Pharmacology

Protein–protein interaction (PPI) networks were constructed using the STRING database (confidence score ≥ 0.7) to identify functional associations among target proteins and visualized in Cytoscape v3.10.3. Network topology analysis was performed using the CytoHubba plugin with four centrality algorithms, Maximal Clique Centrality (MCC), Maximum Neighborhood Component (MNC), Degree, and Closeness, to identify the top 10 hub proteins potentially playing central roles in the underlying biological mechanisms.

Functional Annotation

Functional annotation of key proteins was performed using the DAVID server based on Gene Ontology (Biological Process, Cellular Component, and Molecular Function) and KEGG pathway analyses to identify their biological functions and associated cellular pathways.

Candidate Screening and Drug-Likeness Evaluation

Metabolite features were prioritized based on peak area, structural novelty, and MS/MS fragment quality. Drug-likeness was assessed using SwissADME (http://www.swissadme.ch/) according to Lipinski, Ghose, Veber, Egan, and Muegge criteria. ADMET properties, including absorption, distribution, metabolism, excretion, and toxicity, were predicted using pkCSM (https://biosig.lab.uq.edu.au/pkcsm/) (Pires et al., 2015). Cell membrane permeability was estimated with PerMM (https://permm.phar.umich.edu/) under physiological conditions (310 K, pH 7.4) (Lomize et al., 2019), using energy transfer values and 3D visualization to describe compound orientation across the lipid bilayer. Top candidates were selected for subsequent network and docking analyses.

Molecular Docking

Three-dimensional structures of EGFR wild type (PDB ID: 4WKQ) and the L858R mutant (PDB ID: 6JWL) were retrieved from the RCSB Protein Data Bank (https://www.rcsb.org/). Gefitinib and Osimertinib, standard EGFR inhibitors used in NSCLC therapy, were employed as reference ligands to define the active sites. The selected Langusei compounds targeting EGFR were obtained from PubChem after passing drug-likeness and ADMET screening. Protein preparation was performed in BIOVIA Discovery Studio 2019 by removing water molecules and non-essential ligands. Docking was carried out using AutoDock Vina integrated in PyRx 0.8, with the grid box centered on the native ligand binding site. Validation was conducted by re-docking the co-crystallized ligand, ensuring an RMSD $\leq$ 2.0 Å. Binding affinities and molecular interactions were visualized using BIOVIA Discovery Studio 2019.

RESULTS

Metabolites of Langusei Fruit

Metabolomic profiling of Langusei fruit extracts revealed a highly diverse chemical composition, categorized by compound classes and subclasses (**Figure 1A–D**). At the class level (**Figure 1A**), fatty acyls represented the dominant group, accounting for 25.3% (43 compounds), followed by prenol lipids at 13.53% (23 compounds) and steroids and steroid derivatives at 7.6% (13 compounds). Other notable classes included benzene and substituted derivatives and carboxylic acids and derivatives, each contributing 5.29% (9 compounds), as well as organoxygen compounds (4.71%, 8 compounds), linear 1,3-diarylpropanoids (3.53%, 6 compounds), and glycerolipids (3.53%, 6 compounds).

The other Compounds group (**Figure 1B**) comprised 9.41% of the total 170 metabolites, distributed across 16 single-compound classes such as neoflavonoids, isoquinolines and derivatives, aryltetralin lignans, organic sulfonic acids, tricyclic terpenes, oxazines, and organobromides. Although minor in abundance, these compounds enriched the chemical complexity and indicated substantial secondary metabolite diversity.

At the subclass level (**Figure 1C**), fatty acids and conjugates were predominant (8.82%, 15 compounds), followed by triterpenoids (6.47%, 11 compounds). Additional subclasses such as fatty acid esters, linoleic acid derivatives, amino acids, peptides, and analogues, and sesquiterpenoids each contributed 4.13%, while fatty amides represented 3.53%. The Other

compounds group at the subclass level (**Figure 1D**) encompassed 24.71%, consisting of six unclassified and 36 single-compound subclasses. These included structurally distinctive metabolites such as glycosphingolipids, terpene lactones, prenylated neoflavonoids, unsaturated aliphatic hydrocarbons, and quinoline or hydroquinone lipids, which, despite their low abundance, contributed significantly to the structural and functional diversity of the extract. These results demonstrate that the combined GC–MS and LC–HRMS approach successfully characterized a chemically complex metabolite profile of Langusei fruit, dominated by fatty acyls and fatty acid derivatives, alongside diverse minor components that reflect the species' rich secondary metabolic composition. A total of 170 compounds were identified through LC–HRMS and GC–MS analyses, which may serve as a basis for further studies on the biological potential and pharmacological activities of the extract. The complete list of identified compounds is presented in **Table 1**.

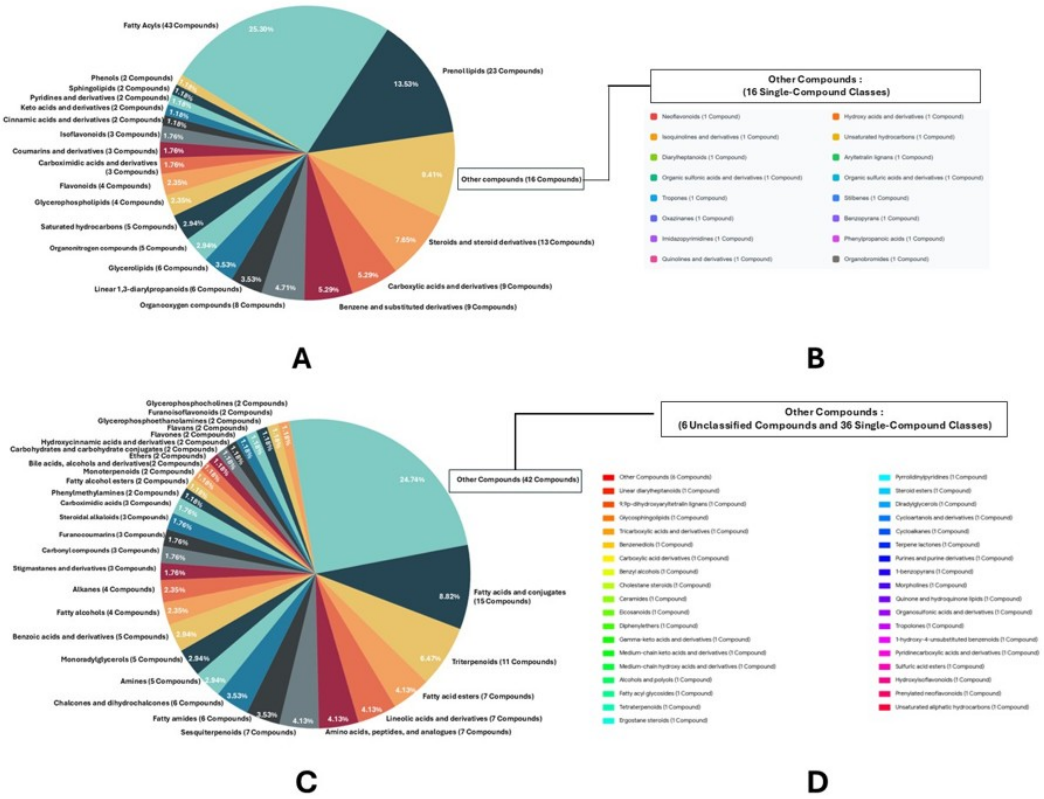


Figure 1. Classification of metabolites identified from GC–MS and LC–HRMS analyses of ethanol and n-hexane extracts. (A) Compound distribution by class showing the dominance of fatty acyls, followed by prenol lipids and steroids and steroid derivatives. (B) The other compounds group at the class level includes several single-compound classes such as neoflavonoids and isoquinolines and derivatives. (C) At the subclass level, fatty acids and conjugates and triterpenoids were predominant. (D) The other compounds group at the subclass level contains minor metabolites such as glycosphingolipids and prenylated neoflavonoids, contributing to the chemical diversity of the extract.

Table 1. List of compounds detected in methanol and n-hexane extracts using LC–HRMS and GC–MS analyses.

Name of Compounds		
Apigenin	Imperialin	sulfobacin A
Arachidic acid	Isofraxidin	Tetracosane, 11-decyl-

Arachidoyl glycine	Isoleucine	Tetradecane, 2,6,10-trimethyl-
Asiatic acid	Isoliquiritigenin	Tetradecanedioic acid
Batilol	Icosanamide	tetranor-12(R)-HETE
behenic acid	Jervine	Tetrapentacontane, 1,54-dibromo-
Benzyl-β-D-glucoside	Leucadenone A	Thapsic acid
beta-Amyrenonol	Licoarylcoumarin	Tocopheryl acetate
Beta-Sitosterol	Linoleamide	trans-13-Octadecenoic acid
Betulin	Linoleic Acid	trans-9-Octadecenoic acid, pentyl ester
Bis(2-ethylhexyl) amine	Linoleic acid, 13-hydroperoxy-, L-	Tribenzylamine
Brasiliensophyllic acid A	Linoleoyl ethanolamide	Tridemorph
Brosimacutin G	Linoleyl alcohol	Vanillic acid
C16-Dihydroceramide	Liquidambaric acid	Visnagin
Calcitriol	Lupeol	Xanthine
Calocarpin	LysoPC(18:3(9Z,12Z,15Z))	Xanthotoxol
Calyxin B	L-α-PALMITIN	α-Linolenic acid
Capsi-amide	Maslinic acid	β-Ionone
Catechol	Monobutyrin	(−)-Cholesteryl acetate
cis-13-Eicosenoic acid	Monoolein	(+)-vulgraon B
Citric acid	Myristyl sulfate	(±)-Abscisic acid
Corchorifatty acid F	Nicotinic acid	(20R)-Cholesta-3,5-diene
Marmesin	N-Methyl-D-aspartic acid (NMDA)	(22E)-Stigmasta-5,22-dien-3-ol
Cycloolivil	Octacosane, 2-methyl-	(E,E)-α-Farnesene
Cyclopentane	Octacosyl (E)-ferulate	(S)-Nicotine
Denticulaflavonol	Octadecane, 3-ethyl-5-(2-ethylbutyl)-	1,2-Dioleoyl-sn-glycerol
Dibenzylamine	Octadecane, 6-methyl-	1,3-DILINOLEIN
Dihydrojasmone	Oleamide	1,5-Isoquinolinediol
dihydrophaseic acid 4-O-β-D-glucoside	Oleanolic acid	17-Pentatriacontene
Docosanamide	Oleic acid	1-Hexadecanol, 2-methyl-
Docosyl 2,3-dihydroxybenzoate	Oleoyl ethanolamide	1-Linoleoyl glycerol
DOCOSYLFERULATE	Orotinichalcone	1-Stearoylglycerol
Dodecylethanol amide	Ovaliflavanone D	1-Tetradecylamine
D-Sphingosine	Palmitoyl ethanolamide	2,4,6-Trihydroxyacetophenone
Echinenone	palmoxiric acid	2,6-Dimethylquinoline
Eicosyl octyl ether	Phenol	24-methylenecycloartanol
Epidihydrophaseic acid	Philanthotoxin 74	2-Hydroxyvaleric acid
Ergosterol peroxide	Pongachalcone II	2-Isopropyl-5-methyl-1-heptanol
Erucic acid	Prednisolone farnesylate	2-Methylglutaric acid
Ethanol, 2-(9-octadecenyloxy)-, (Z)-	Psoralen	2-Oxoglutaric acid
Ethyl iso-allocholate	Purpurogallin	3-Anisic acid
Ethyl myristate	Resveratrol	3-Epicorosolic acid
Gentisic acid	rhuscholide A	3-Hydroxybenzoic acid
Geranyl caproate	Ricinoleic Acid	3-Hydroxybenzyl alcohol
Geranylacetone	Rosin	3-Hydroxydecanoic acid
Glycidyl oleate	Salidroside	4',7-Dihydroxy-8-prenylflavanone

Glycocholic acid	Squalene	4-Hydroxybenzaldehyde
Hexadecanamide	Stearamide	4-oxododecanedioic acid
Hexadecanedioic acid	Stearic acid	4-Oxoproline
Isoliquiritigenin 4-methyl ether	Stigmasta-3,5-diene	5-Aminovaleric acid
(18R)-24-Amino-21-hydroxy-21-oxido-15-oxo-16,20,22-trioxa-21λ~5~-phosphatetracosan-18-yl (9Z)-9-octadecenoate	(2E,4E,14E)-13-Hydroperoxy-N-(2-methylpropyl)icosa-2,4,14-trienamide	(2R)-1-{[(2-Aminoethoxy)(hydroxy)phosphoryl]oxy}-3-hydroxy-2-propanyl tetracosanoate
(2R)-2-Amino-3-[(hydroxy{[(2S,3R)-2-{[(9Z)-9-octadecenoyloxy]methyl}tetrahydro-2H-pyran-3-yl]oxy}phosphoryl)oxy]propanoic acid (non-preferred name)	(2R)-N-[(2S,3R,4E)-1,3-Dihydroxy-4-octadecen-2-yl]-2-hydroxytetracosanamide	(2R)-N-[(2S,3S,4R)-1-(D-Glucopyranosyloxy)-3,4-dihydroxy-8-octadecen-2-yl]-2-hydroxyhexadecanamide
Oleic acid, 3-(octadecyloxy)propyl ester	Oxiraneundecanoic acid, 3-pentyl-, methyl ester, trans-	10-Octadecenoic acid, methyl ester
1-Palmitoyl-2-linoleoyl-sn-glycero-3-PC	25-Norisopropyl-9,19-cyclolanostan-22-en-24-one, 3-acetoxy-24-phenyl-4,4,14-trimethyl-	(*Z*)-1-(1,3-benzodioxol-5-yl)-3-methoxy-3-(2,4,6-trimethoxyphenyl)prop-2-en-1-one
3-[4-methyl-1-(2-methylpropanoyl)-3-oxocyclohexyl]butanoic acid	7-Methyl-Z-tetradecen-1-ol acetate	(2S)-1-Hydroxy-3-(pentadecanoyloxy)-2-propanyl (9Z,12Z,15Z)-9,12,15-octadecatrienoate
9-Octadecenoic acid (Z)-, 2-hydroxy-1-(hydroxymethyl)ethyl ester	9S,13R-12-Oxophytodienoic acid	Cyclopropanebutanoic acid, 2-[[2-[[2-[(2-pentylcyclopropyl)methyl]cyclopropyl]methyl]cyclopropyl]methyl]-, methyl ester
2-Hydroxy-6-[2-hydroxy-6-(hydroxymethyl)-4-methyl-phenoxy]-3-(3-methylbut-2-enyl)benzoic acid	9-methoxy-6a,11a-dihydro-6H-(1)benzofuro(3,2-c)chromen-3-ol)	

Target Protein Prediction

Protein target prediction identified 132 targets using SwissTargetPrediction and 337 targets using the Similarity Ensemble Approach (SEA). Integration with NSCLC-related databases revealed varying numbers of disease-associated targets: OMIM (187), GeneCards (27,271), Gepia2 (12,501), DisGeNET (276), and cBioPortal (1,181). These results formed the basis for selecting relevant proteins for subsequent network construction and functional annotation (**Figure 2**).

To obtain more specific candidate proteins, an intersection analysis was performed between the predicted protein targets of Langusei compounds (from SwissTargetPrediction and SEA) and proteins associated with non-small cell lung cancer (NSCLC) based on database integration. The overlapping targets were visualized using a Venn diagram to identify proteins with higher biological and clinical relevance to NSCLC (**Figure 3**).

Network Pharmacology

Protein–protein interaction (PPI) analysis identified a high-confidence interaction network among the predicted target proteins using the STRING database (confidence score ≥ 0.7). The resulting network served as the basis for topological analysis (**Figure 4**).

CytoHubba analysis identified ten key hub proteins based on four complementary centrality algorithms (MCC, MNC, Degree, and Closeness), highlighting the most influential proteins within the network for subsequent analyses (**Figure 5**).



Figure 2. Number of predicted protein targets obtained using SwissTargetPrediction and the Similarity Ensemble Approach (A). Distribution of NSCLC-related protein targets retrieved from five databases: OMIM (187), GeneCards (27,271), Gepia2 (12,501), DisGeNET (276), and cBioPortal (1,181) (B). A logarithmic scale was applied to enhance visualization of differences among the databases.

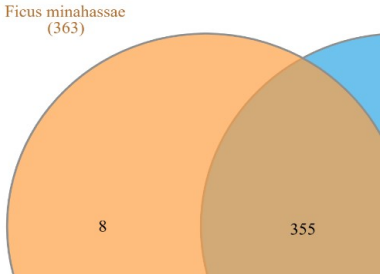


Figure 3. Venn diagram showing the overlap between predicted protein targets of Langusei compounds (identified through SwissTargetPrediction and the Similarity Ensemble Approach [SEA]) and proteins associated with non-small cell lung cancer (NSCLC).

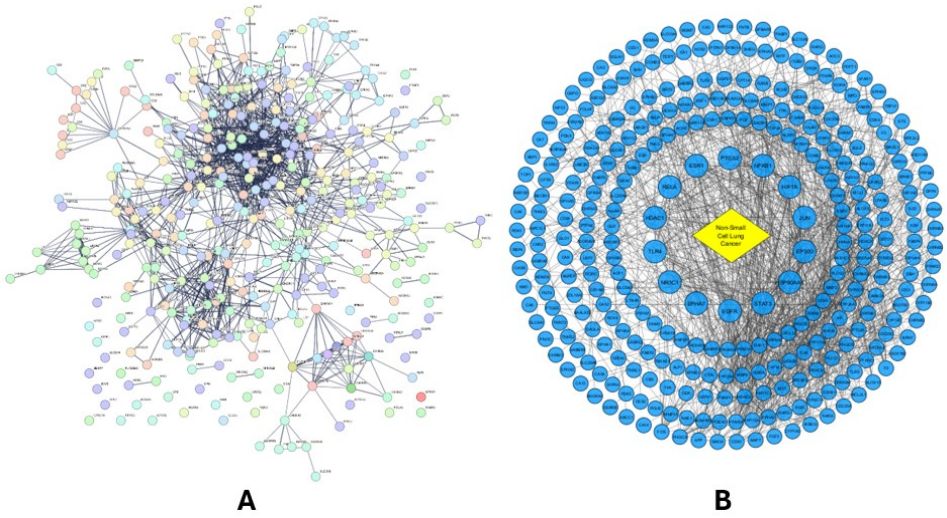


Figure 4. Protein–protein interaction (PPI) network of targets associated with non-small cell lung cancer (NSCLC). (**A**) PPI network generated using STRING with a high-confidence score (≥0.7). (**B**) Refined PPI network after filtering out proteins that did not interact with the main network.

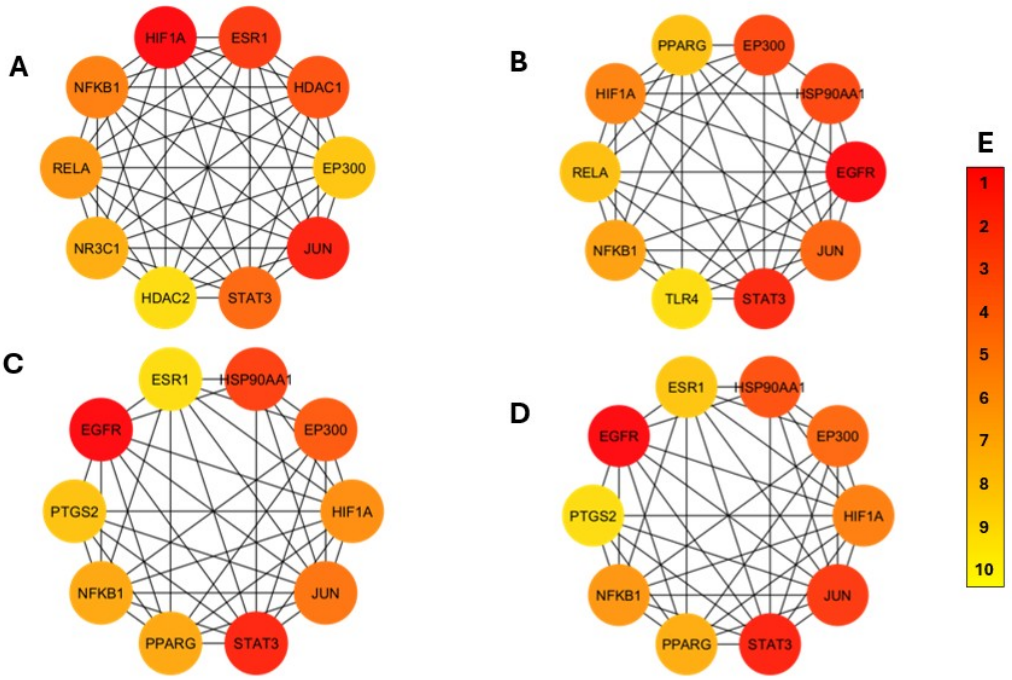


Figure 5. Hub protein analysis of non-small cell lung cancer (NSCLC) using CytoHubba. Each algorithm identified the top 10 proteins with the highest centrality scores, indicating variations in key proteins that may serve as potential molecular targets. (A) Maximal Clique Centrality (MCC) algorithm, (B) Maximum Neighborhood Component (MNC) algorithm, (C) Degree algorithm, and (D) Closeness algorithm. (E) The color scale represents node ranking based on centrality values.

Network topology analysis using four centrality algorithms identified several proteins with the highest centrality scores (**Table 2**). For consistency, the top three proteins from each algorithm were selected. Proteins recurring across multiple algorithms were given particular attention, as their consistent appearance suggests stronger topological importance within the PPI network. This approach identified seven key candidates: EGFR, STAT3, EP300, HSP90AA1, JUN, HIF1A, and ESR1. These proteins ranked highly in more than one algorithm, reinforcing their status as potential hub nodes. Consequently, they were selected for further Gene Ontology (GO) and KEGG pathway analyses to elucidate their involvement in the molecular mechanisms of non-small cell lung cancer (NSCLC).

Table 2. Top ten proteins identified using the MCC, MNC, Degree, and Closeness algorithms in the PPI network analysis.

Algorithm							
MCC	**Value**	**MNC**	**Value**	**Degree**	**Value**	**Closeness**	**Value**
HIF1A	4554016.0	EGFR	48.0	EGFR	52.0	EGFR	151.88
JUN	4553692.0	STAT3	41.0	STAT3	44.0	STAT3	143.08
ESR1	4537963.0	EP300	36.0	HSP90AA1	38.0	JUN	141.12
HDAC1	4521756.0	HSP90AA1	36.0	EP300	37.0	HSP90AA1	137.93

STAT3	4519465.0	JUN	35.0	JUN	35.0	EP300	137.62
NFKB1	4472790.0	HIF1A	30.0	HIF1A	32.0	HIF1A	136.83
RELA	4459200.0	NFKB1	29.0	NFKB1	29.0	NFKB1	135.07
NR3C1	4084203.0	PPARG	27.0	PPARG	29.0	PPARG	134.86
EP300	4079295.0	RELA	27.0	PTGS2	28.0	ESR1	133.05
HDAC2	4032328.0	TLR4	26.0	ESR1	27.0	PTGS2	131.66

Functional Annotation

The seven key proteins identified from network topology analysis were further examined through functional annotation using a false discovery rate (FDR) cut-off of 0.05 to ensure biological significance. In the Gene Ontology (GO) database, proteins were classified into three main domains: Biological Process (BP), Cellular Component (CC), and Molecular Function (MF). KEGG pathway analysis was then performed to map their involvement in relevant cellular pathways. Overall, the annotation results provide insights into the biological roles of these key proteins within cellular processes and molecular pathways. The visualization (**Figure 6**) illustrates the KEGG pathway mapping and GO category distribution based on significance and the number of proteins involved.

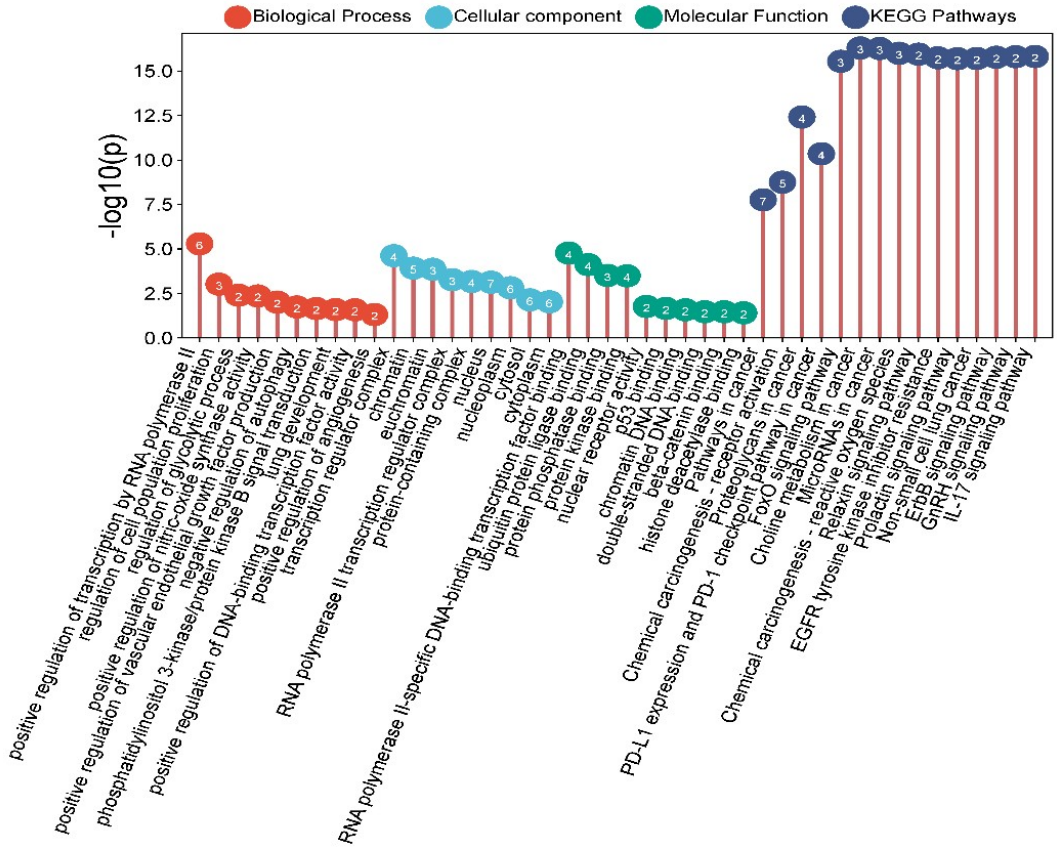


Figure 6. Functional annotation of key proteins associated with non-small cell lung cancer (NSCLC), showing Gene Ontology (GO) classification across Biological Process (BP), Cellular Component (CC), and Molecular Function (MF) domains, as well as KEGG pathway enrichment illustrating significant cellular pathways involving the identified proteins (FDR < 0.05).

The complete results of the KEGG pathway enrichment are presented in **Table 3**, which lists the KEGG IDs, pathway names, and proteins involved. The seven key proteins (EGFR, STAT3, JUN, HSP90AA1, EP300, HIF1A, and ESR1) were mapped to multiple signaling pathways associated with cancer development, progression, and therapeutic resistance. The pathway "hsa05200: Pathways in cancer" included all seven proteins, reflecting their broad regulatory roles in oncogenic signaling networks.

Table 3. KEGG pathways enriched with the seven key proteins (EGFR, STAT3, JUN, HSP90AA1, EP300, HIF1A, and ESR1) identified from network analysis.

KEGG ID	Pathways	Genes
hsa05200	Pathways in cancer	HSP90AA1, JUN, STAT3, EP300, ESR1, HIF1A, EGFR
hsa05207	Chemical carcinogenesis - receptor activation	HSP90AA1, JUN, STAT3, ESR1, EGFR
hsa05205	Proteoglycans in cancer	STAT3, ESR1, HIF1A, EGFR
hsa05235	PD-L1 expression and PD-1 checkpoint pathway in cancer	JUN, STAT3, HIF1A, EGFR
hsa04068	FoxO signaling pathway	STAT3, EP300, EGFR
hsa05231	Choline metabolism in cancer	JUN, HIF1A, EGFR
hsa05206	MicroRNAs in cancer	STAT3, EP300, EGFR
hsa05208	Chemical carcinogenesis - reactive oxygen species	JUN, HIF1A, EGFR
hsa04926	Relaxin signaling pathway	JUN, EGFR
hsa01521	EGFR tyrosine kinase inhibitor resistance	STAT3, EGFR
hsa04917	Prolactin signaling pathway	STAT3, ESR1
hsa05223	Non-small cell lung cancer	STAT3, EGFR
hsa04012	ErbB signaling pathway	JUN, EGFR
hsa04912	GnRH signaling pathway	JUN, EGFR
hsa04657	IL-17 signaling pathway	HSP90AA1, JUN

Among them, EGFR and STAT3 appeared most frequently across diverse cancer-related pathways, including proteoglycans in cancer (hsa05205), PD-L1 expression and PD-1 checkpoint pathway in cancer (hsa05235), and FoxO signaling (hsa04068), emphasizing their roles in tumor proliferation, immune evasion, and cell survival. The presence of EGFR tyrosine kinase inhibitor resistance (hsa01521) and non-small cell lung cancer (hsa05223) pathways highlights their direct relevance to NSCLC pathogenesis and therapeutic resistance. Moreover, pathways such as ErbB signaling (hsa04012) and choline metabolism in cancer (hsa05231) further demonstrate the interconnected functions of EGFR and its co-regulators in cancer signaling. The analysis results were also mapped and visualized to illustrate the biological context of the identified proteins, particularly their involvement in general cancer pathways (**Figure 7**) and specifically in non-small cell lung cancer (**Figure 8**).

The relationships between the identified active compounds and their target proteins are summarized in **Table 4**, highlighting the associations between key proteins from the KEGG pathway analysis and putative bioactive metabolites predicted to modulate cancer-related pathways. Notably, (Z)-1-(1,3-benzodioxol-5-yl)-3-methoxy-3-(2,4,6-trimethoxyphenyl)prop-2-en-1-one (syn. 3′,4′-methylenedioxy-2,4,6-β-tetramethoxychalcone), a chalcone-type flavonoid derived from the polyketide pathway, exhibited strong predicted interactions with EGFR and STAT3, two key regulatory proteins in the molecular network of non-small cell lung cancer (NSCLC).

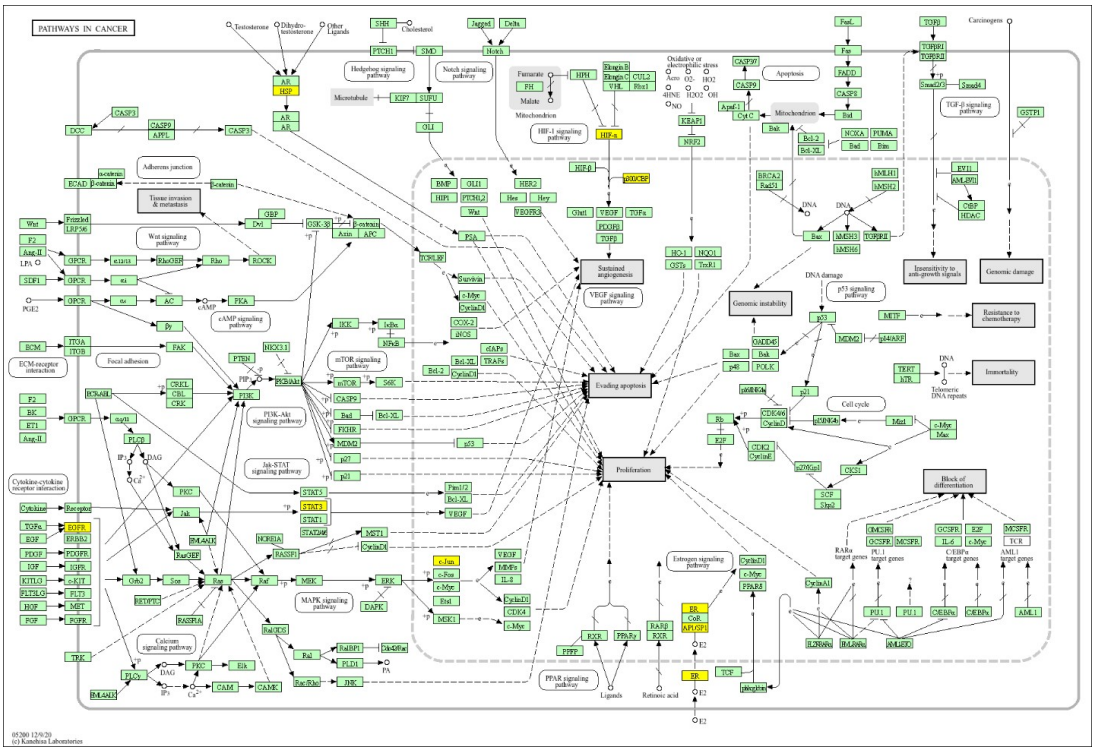


Figure 7. KEGG pathway map for "Pathways in cancer," with the identified proteins highlighted as yellow-colored nodes. The visualization was generated using KEGG Mapper (https://www.genome.jp/kegg/mapper.html).

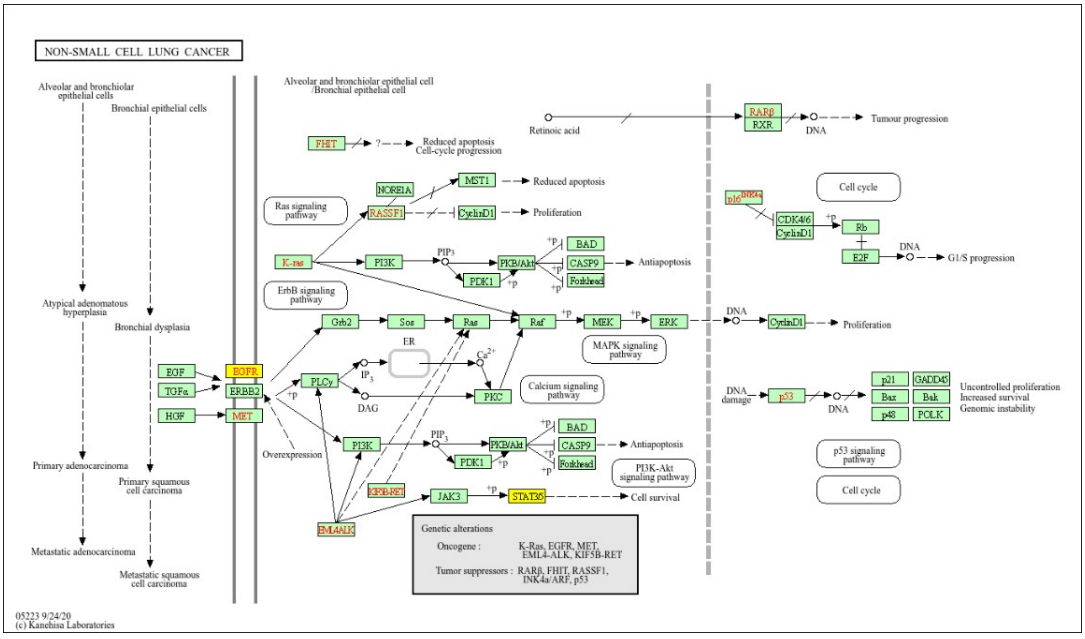


Figure 8. KEGG pathway map for "Non-small cell lung cancer," with the identified proteins highlighted as yellow-colored nodes. The visualization was generated using KEGG Mapper (https://www.genome.jp/kegg/mapper.html).

Table 4. Associations between key proteins identified from KEGG pathway analysis and putative bioactive compounds, including EGFR and STAT3, which play crucial roles in non-small cell lung cancer (NSCLC).

Protein	Compound
EGFR	(*Z*)-1-(1,3-benzodioxol-5-yl)-3-methoxy-3-(2,4,6-trimethoxyphenyl)prop-2-en-1-one
STAT3	(*Z*)-1-(1,3-benzodioxol-5-yl)-3-methoxy-3-(2,4,6-trimethoxyphenyl)prop-2-en-1-one
EP300	(*Z*)-1-(1,3-benzodioxol-5-yl)-3-methoxy-3-(2,4,6-trimethoxyphenyl)prop-2-en-1-one, Docosylferulate, Octacosyl (e)-ferulate
HSP90AA1	Isoliquiritigenin 4-methyl ether
JUN	(*Z*)-1-(1,3-benzodioxol-5-yl)-3-methoxy-3-(2,4,6-trimethoxyphenyl)prop-2-en-1-one, Docosylferulate, Octacosyl (e)-ferulate
HIF1A	Marmesin
ESR1	Resveratrol, Apigenin

Candidate Screening and Drug-Likeness Evaluation

Previous KEGG pathway and protein–protein interaction analyses identified seven key proteins involved in cancer and NSCLC. The corresponding bioactive compounds were subsequently evaluated for drug-likeness criteria (**Table 5**). The results showed that most compounds met all major pharmacokinetic parameters, indicating favorable oral bioavailability. (Z)-1-(1,3-benzodioxol-5-yl)-3-methoxy-3-(2,4,6-trimethoxyphenyl)prop-2-en-1-one, isoliquiritigenin 4-methyl ether, resveratrol, apigenin, and marmesin exhibited no violations across all rule sets, suggesting strong drug-like potential. In contrast, docosylferulate and octacosyl (E)-ferulate showed multiple violations, primarily due to their high molecular weights and lipophilicity, indicating lower drug-likeness and possible limitations in absorption.

Table 5. Drug-likeness evaluation of candidate compounds according to the Lipinski, Ghose, Veber, Egan, and Muegge criteria.

Compounds	MW	Lipinski #violations	Ghose #violations	Veber #violations	Egan #violations	Muegge #violations
(*Z*)-1-(1,3-benzodioxol-5-yl)-3-methoxy-3-(2,4,6-trimethoxyphenyl)prop-2-en-1-one	371.37	0	0	0	0	0
Docosylferulate	502.77	2	4	1	1	2
Octacosyl (e)-ferulate	586.93	2	4	1	1	2
Isoliquiritigenin 4-methyl ether	270.28	0	0	0	0	0
Resveratrol	228.24	0	0	0	0	0
Apigenin	270.24	0	0	0	0	0
Marmesin	246.26	0	0	0	0	0

The ADMET profiling analysis (**Table 6**) provided a detailed assessment of the pharmacokinetic and toxicity-related characteristics of the candidate compounds, including parameters of absorption, distribution, metabolism, excretion, and toxicity. Most compounds demonstrated favorable absorption properties, with high Caco-2 permeability values (>1.0 log Papp) and intestinal absorption rates above 84%, indicating good bioavailability potential.

Among them, (Z)-1-(1,3-benzodioxol-5-yl)-3-methoxy-3-(2,4,6-trimethoxyphenyl)prop-2-en-1-one, marmesin, apigenin, and isoliquiritigenin 4-methyl ether showed the highest predicted intestinal absorption (>93%) and acceptable water solubility, suggesting strong pharmacokinetic compatibility. These compounds also exhibited moderate skin permeability (log Kp ≈ −2.7 to −3.1), consistent with good membrane diffusion.

Table 6. ADMET profiling of candidate compounds, including predicted parameters of absorption, distribution, metabolism, excretion, and toxicity, to evaluate pharmacokinetic suitability and potential drug-likeness.

Compounds	Absorption						
	Water solubility (log mol/L)	Caco2 permeability (log Papp in 10^{-6} cm/s)	Intestinal absorption (human) (%)	Skin Permeability (log Kp)	P-glycoprotein substrate	P-glycoprotein I inhibitor	P-glycoprotein II inhibitor
(*Z*)-1-(1,3-benzodioxol-5-yl)-3-methoxy-3-(2,4,6-trimethoxyphenyl)prop-2-en-1-one	-5.43	1.278	96.137	-2.746	No	Yes	Yes
Docosylferulate	-5.302	1.234	86.197	-2.734	No	No	Yes
Octacosyl (e)-ferulate	-4.036	1.207	84.135	-2.735	No	No	Yes
Isoliquiritigenin 4-methyl ether	-3.16	1.003	93.008	-2.819	Yes	No	No
Resveratrol	-3.178	1.17	90.935	-2.737	Yes	No	No
Apigenin	-3.329	1.007	93.25	-2.735	Yes	No	No
Marmesin	-3.136	1.155	96.484	-3.128	No	No	No

Resveratrol and apigenin were predicted to be P-glycoprotein substrates, which may influence their efflux and bioavailability, whereas (Z)-1-(1,3-benzodioxol-5-yl)-3-methoxy-3-(2,4,6-trimethoxyphenyl)prop-2-en-1-one acted as a dual P-glycoprotein inhibitor, suggesting potential effects on drug transport modulation. In contrast, docosylferulate and octacosyl (E)-ferulate displayed slightly lower absorption values (<87%) and reduced solubility due to their larger molecular size and lipophilicity, indicating limited pharmacokinetic suitability.

The ADMET screening for distribution and metabolism parameters (**Table 7**) revealed that most compounds exhibit favorable pharmacokinetic characteristics with limited blood–brain barrier (BBB) permeability, suggesting selective distribution in peripheral tissues rather than the central nervous system (CNS). All compounds showed low to moderate volume of distribution (VDss, log Kp ranging from −0.52 to 0.82) and generally low fraction unbound (Fu < 0.4), indicating moderate plasma protein binding.

Marmesin displayed the highest BBB permeability (log BB = 0.386), suggesting potential CNS access, whereas other compounds such as (Z)-1-(1,3-benzodioxol-5-yl)-3-methoxy-3-(2,4,6-trimethoxyphenyl)prop-2-en-1-one and octacosyl (E)-ferulate showed negative log BB values, implying minimal CNS penetration. Regarding metabolic stability, most compounds were predicted as CYP3A4 substrates, indicating metabolism primarily through this major hepatic enzyme. Only isoliquiritigenin 4-methyl ether and (Z)-1-(1,3-

benzodioxol-5-yl)-3-methoxy-3-(2,4,6-trimethoxyphenyl)prop-2-en-1-one were identified as CYP2C9 inhibitors, while isoliquiritigenin 4-methyl ether also inhibited CYP3A4, suggesting possible drug–enzyme interactions.

Table 7. ADMET screening results for distribution and metabolism parameters of candidate compounds, including predicted values for volume of distribution (VDss), plasma protein binding (fraction unbound), blood–brain barrier (BBB) and CNS permeability, as well as CYP enzyme substrate and inhibition profiles.

Compounds	Distribution				Metabolism				
	VDss (human) (log Kp)	Fraction un-bound (human) (Fu)	BBB perme-ability (log BB)	CNS perme-ability (log PS)	CYP2 D6 sub-strate	CYP3 A4 sub-strate	CYP2 C9 inhibi-tion	CYP2 D6 inhibi-tion	CYP3 A4 inhibi-tion
(*Z*)-1-(1,3-benzodioxol-5-yl)-3-methoxy-3-(2,4,6-trimethoxyphenyl)prop-2-en-1-one	-0.446	0	-0.936	-3.043	No	Yes	Yes	No	No
Docosylferulate	-0.026	0.044	-0.789	-2.61	No	Yes	No	No	No
Octacosyl (e)-ferulate	-0.522	0.141	-1.041	-2.659	No	Yes	No	No	No
Isoliquiritigenin 4-methyl ether	0.134	0.049	-0.326	-2.248	No	Yes	Yes	No	Yes
Resveratrol	0.296	0.166	-0.048	-2.067	No	Yes	No	No	No
Apigenin	0.822	0.147	-0.734	-2.061	No	No	No	No	No
Marmesin	0.507	0.361	0.386	-2.824	No	No	No	No	No

The excretion and toxicity screening (**Table 8**) showed that most candidate compounds exhibited favorable pharmacokinetic and safety profiles. Predicted total clearance values ranged from 0.07 to 1.67 log mL/min/kg, suggesting moderate elimination rates suitable for maintaining systemic exposure. None of the compounds were predicted as renal OCT2 substrates, indicating low risk of renal transporter-related drug interactions.

In terms of toxicity, all compounds were predicted to be non-hepatotoxic and non–skin-sensitizing, reflecting a low likelihood of hepatic or dermatological adverse effects. Moreover, none were identified as hERG I inhibitors, implying minimal risk of cardiotoxicity related to QT prolongation. Only a few compounds, such as docosylferulate, octacosyl (E)-ferulate, and isoliquiritigenin 4-methyl ether, showed weak potential as hERG II inhibitors, which may warrant further monitoring in later testing stages.

Membrane permeability was simulated under physiological conditions (310 K, pH 7.4) to assess the ability of each compound to traverse the lipid bilayer. Variations in free energy (ΔG) profiles indicated distinct permeation potentials among the tested molecules (**Figure 9**). Chalcone-type compounds such as (Z)-1-(1,3-benzodioxol-5-yl)-3-methoxy-3-(2,4,6-trimethoxyphenyl)prop-2-en-1-one and apigenin exhibited moderate ΔG minima, suggesting favorable lipid bilayer penetration, whereas long-chain ferulate esters (docosylferulate and

octacosyl (E)-ferulate) showed higher energy barriers, implying lower membrane permeability.

Table 8. ADMET screening results for excretion and toxicity parameters of candidate compounds, including predicted total clearance, renal OCT2 substrate status, and potential toxicological effects such as hERG inhibition, hepatotoxicity, and skin sensitization

Compounds	Excretion		Toxicity				
	Total Clearance (log ml/min/kg)	Renal OCT2 sub-strate	Max. tolerated dose (human) (log mg/kg/day)	hERG I inhibi-tor	hERG II inhibi-tor	Hepatoto-xicity	Skin Sensitis-ation
(*Z*)-1-(1,3-benzodioxol-5-yl)-3-methoxy-3-(2,4,6-trimethoxyphenyl)prop-2-en-1-one	0.682	No	0.839	No	No	No	No
Docosylferulate	1.619	No	0.215	No	Yes	No	No
Octacosyl (e)-ferulate	1.668	No	0.179	No	Yes	No	No
Isoliquiritigenin 4-methyl ether	0.126	No	0.027	No	Yes	No	No
Resveratrol	0.076	No	0.331	No	No	No	No
Apigenin	0.566	No	0.328	No	No	No	No
Marmesin	0.647	No	0.272	No	No	No	No

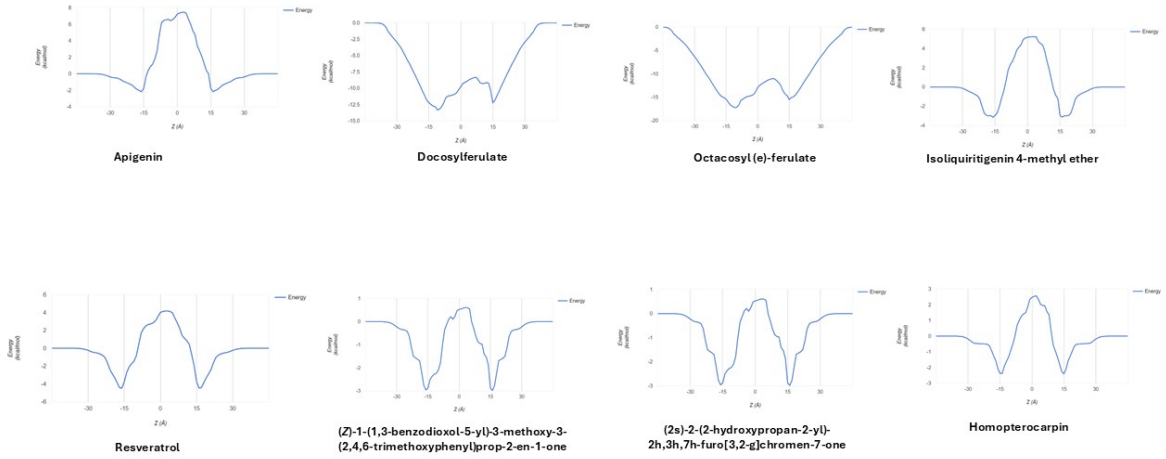


Figure 9. Free energy (ΔG) profiles showing differences in membrane permeability among Langusei compounds. Chalcone-type molecules such as (Z)-1-(1,3-benzodioxol-5-yl)-3-methoxy-3-(2,4,6-trimethoxyphenyl)prop-2-en-1-one and apigenin exhibited moderate ΔG minima, indicating favorable bilayer penetration, while long-chain ferulate esters (docosylferulate and octacosyl (E)-ferulate) displayed higher energy barriers, suggesting lower permeability.

Three-dimensional visualization further illustrated the spatial orientation of each molecule within the lipid bilayer, supporting the energy profile findings and revealing interactions with both hydrophobic and hydrophilic membrane regions (**Figure 10**). Chalcone-type flavonoids, particularly (Z)-1-(1,3-benzodioxol-5-yl)-3-methoxy-3-(2,4,6-

trimethoxyphenyl)prop-2-en-1-one and apigenin, penetrated more deeply into the membrane's hydrophobic core, consistent with their favorable permeability profiles. In contrast, long-chain ferulate esters such as docosylferulate and octacosyl (E)-ferulate remained closer to the membrane surface, suggesting limited diffusion across the bilayer due to their high molecular size and lipophilicity. These results indicate that smaller, moderately lipophilic flavonoids are more likely to traverse lipid membranes effectively than bulkier ferulate derivatives.

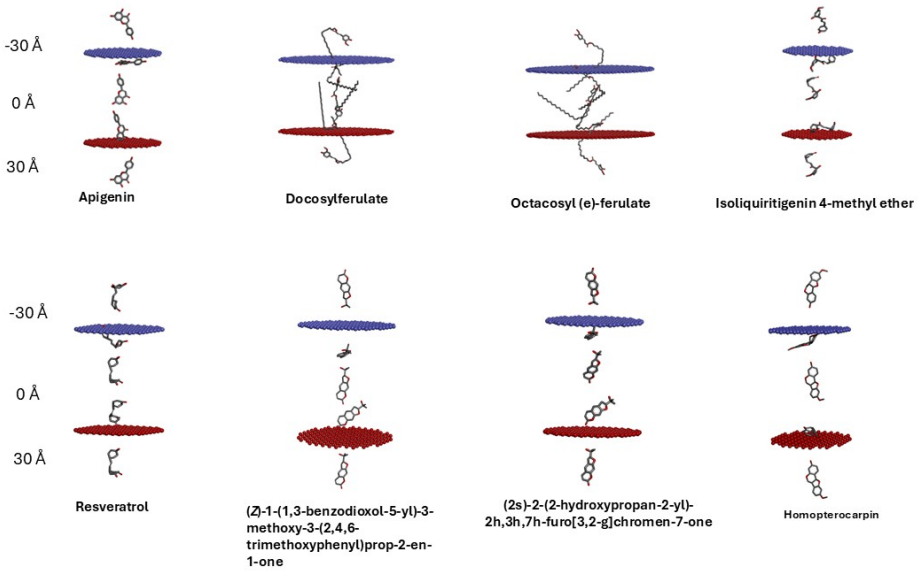


Figure 10. Three-dimensional visualization of compound penetration across the lipid bilayer. The models depict the orientation and depth of insertion of each molecule within the membrane. Chalcone-type flavonoids such as (Z)-1-(1,3-benzodioxol-5-yl)-3-methoxy-3-(2,4,6-trimethoxyphenyl)prop-2-en-1-one and apigenin exhibit deeper insertion into the hydrophobic core, whereas long-chain ferulate esters (docosylferulate and octacosyl (E)-ferulate) remain near the surface, indicating reduced membrane permeability.

Molecular Docking

Molecular docking was conducted to assess the binding affinity of (Z)-1-(1,3-benzodioxol-5-yl)-3-methoxy-3-(2,4,6-trimethoxyphenyl)prop-2-en-1-one against both wild-type EGFR and its L858R mutant. Gefitinib and Osimertinib, clinically approved EGFR inhibitors for non-small cell lung cancer (NSCLC), served as reference ligands for the wild-type and mutant EGFR, respectively. The binding affinities of each complex are summarized in **Table 9**. The docking results demonstrated that the Langusei compound exhibited strong and comparable binding affinities toward both EGFR wild type (–6.8 kcal/mol) and L858R mutant (–6.9 kcal/mol), approaching those of Gefitinib (–7.9 and –7.1 kcal/mol) and Osimertinib (–7.4 and –7.4 kcal/mol). The small difference in binding energy indicates similar interaction stability within the active site, suggesting that this chalcone-type flavonoid could form stable complexes with both EGFR forms and holds potential as a natural EGFR inhibitor candidate for NSCLC therapy.

The molecular docking analysis (**Figure 11**) revealed that chalcone compound, (Z)-1-(1,3-benzodioxol-5-yl)-3-methoxy-3-(2,4,6-trimethoxyphenyl)prop-2-en-1-one, established stable interactions within the EGFR wild-type binding pocket through two key hydrogen bonds with Ala743 and Met793, supported by π–π stacking and van der Waals interactions with adjacent hydrophobic residues. These interactions positioned the compound in a conformation comparable to that of clinically used EGFR inhibitors. In contrast, Gefitinib, the

native ligand, formed multiple hydrogen bonds, including a strong hinge interaction with Met793, consistent with its canonical binding mode, while Osimertinib displayed a similar pattern involving hydrogen and π–alkyl interactions that stabilized the complex within the catalytic pocket. These results indicate that the Langusei chalcone shares a similar binding orientation and interaction profile with Gefitinib and Osimertinib, supporting its potential as a natural inhibitor capable of targeting the EGFR active site.

Table 9. Binding-free energy (kcal/mol) of the interaction of (Z)-1-(1,3-benzodioxol-5-yl)-3-methoxy-3-(2,4,6-trimethoxyphenyl)prop-2-en-1-one and reference inhibitors (Gefitinib and Osimertinib) against EGFR wild type and L858R mutant.

Compounds	Binding Affinity (Kcal/mol)	
	EGFR Wild Type	EGFR L858R
(*Z*)-1-(1,3-benzodioxol-5-yl)-3-methoxy-3-(2,4,6-trimethoxyphenyl)prop-2-en-1-one	-6.8	-6.9
Gefitinib	-7.9	-7.1
Osimertinib	-7.4	-7.4

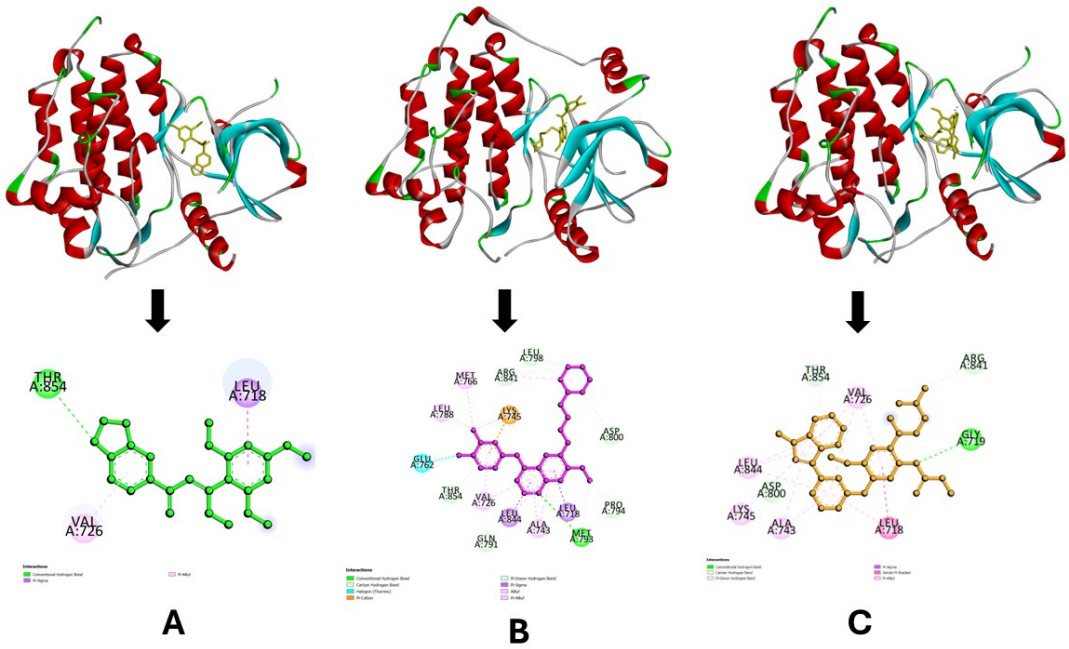


Figure 11. Molecular interaction visualization of compounds bound to EGFR wild type: (A) (Z)-1-(1,3-benzodioxol-5-yl)-3-methoxy-3-(2,4,6-trimethoxyphenyl)prop-2-en-1-one, (**B**) Gefitinib, and (**C**) Osimertinib. The Langusei compound formed stable hydrogen bonds with key residues (Ala743, Met793), showing a binding orientation comparable to the reference inhibitors.

The molecular interaction analysis of the EGFR L858R mutant (**Figure 12**) demonstrated that the *Ficus minahassae* chalcone, (Z)-1-(1,3-benzodioxol-5-yl)-3-methoxy-3-(2,4,6-trimethoxyphenyl)prop-2-en-1-one, formed stable hydrogen bonds with key residues Ala743 and Met793, along with hydrophobic contacts involving Val726 and Leu788, stabilizing the ligand within the mutant receptor's binding cleft. In comparison, Gefitinib displayed multiple hydrogen bonds and π–π stacking interactions with Lys745, Asp855, and Met793, reflecting its canonical hinge-binding configuration. Meanwhile, Osimertinib exhibited hydrogen bonding with Cys797 and Met793 and hydrophobic interactions with Leu718 and Ala743, consistent with its strong inhibitory activity against the L858R mutation.

This shows that Langusei compound showed a similar binding orientation and interaction network to those of Gefitinib and Osimertinib, suggesting that it may effectively engage the EGFR L858R mutant active site with a stable and energetically favorable conformation.

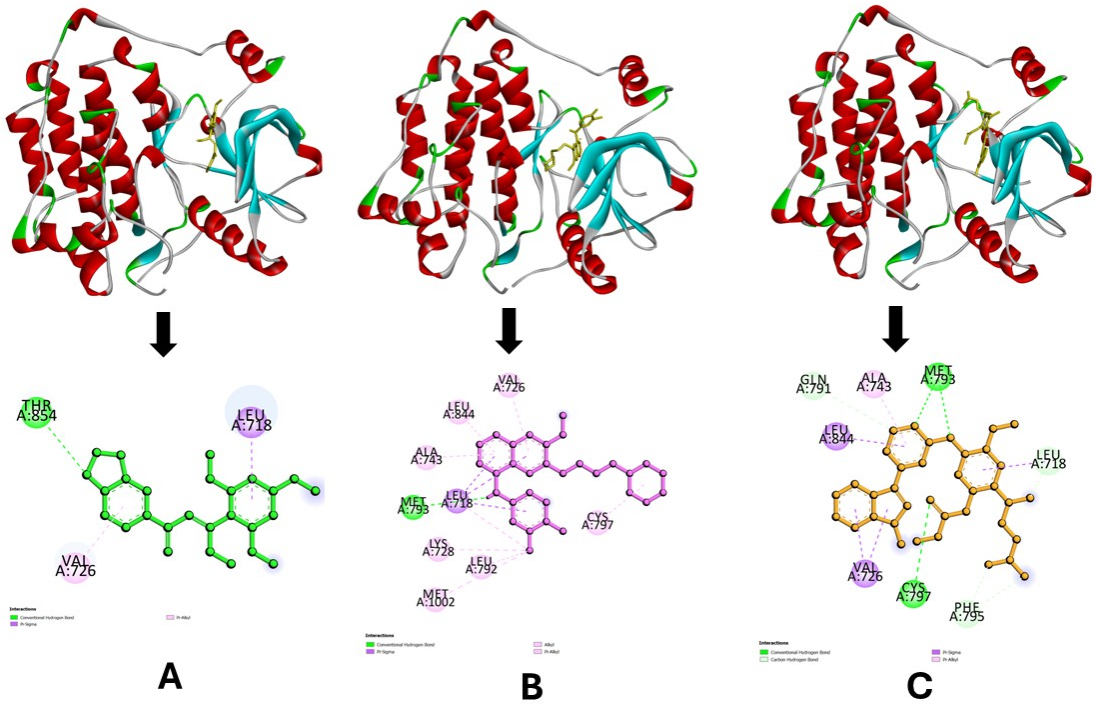


Figure 12. Molecular interaction visualization of compounds bound to the EGFR L858R mutant: (**A**) (Z)-1-(1,3-benzodioxol-5-yl)-3-methoxy-3-(2,4,6-trimethoxyphenyl)prop-2-en-1-one, (**B**) Gefitinib, and (C) Osimertinib. The Langusei compound formed hydrogen bonds with Ala743 and Met793 and hydrophobic contacts with Val726 and Leu788, showing a binding orientation comparable to the reference inhibitors within the mutant EGFR active site.

DISCUSSION

Untargeted metabolomic profiling of *Ficus minahassae* (Langusei) fruit extract using ethanol and n-hexane, analyzed through complementary GC–MS and LC–HRMS platforms, identified 170 metabolites. The profile was dominated by fatty acyls, prenol lipids, and steroid derivatives, reflecting high biochemical complexity consistent with metabolomic patterns observed across the Ficus genus. This dual-platform approach effectively captured both volatile and semi-polar compounds, enabling a comprehensive assessment of secondary metabolites (Salem et al., 2022; Cannavacciuolo et al., 2023).

Similar to other Ficus species, Langusei contains abundant flavonoids, phenolics, terpenoids, and alkaloids, which are compound classes frequently associated with antioxidant and anticancer activities (Cabanlit et al., 2025). Previous phytochemical investigations on *F. minahassae* leaves identified 2-hydroxyethyl benzoate, phytyl fatty acid ester, squalene, and β-sitosterol in dichloromethane extracts (Apostol et al., 2016), further supporting its pharmacological potential.

To date, no prior study has reported *Ficus*-derived metabolites with inhibitory activity against the EGFR wild type or its L858R mutant implicated in NSCLC. However, related evidence exists: a fatty-acid glucoside from *F. benghalensis* was shown to inhibit the EGFR/Akt/PI3K pathway in anti-inflammatory models (Alaaeldin et al., 2022); metabolites from *F. virens* have been screened *in silico* against EGFR without mutant specificity

(Alqurashi et al., 2024); and several chalcone scaffolds, chemically related to the compound identified here, have demonstrated inhibition of both EGFR^WT and EGFR^L858R/T790M in other contexts (Sangpheak et al., 2024). Furthermore, a recent review summarized the broad anticancer potential of *Ficus* species but provided no evidence for EGFR-mutant targeting (Cabanlit et al., 2025). These observations highlight the novelty of the present finding, suggesting that Langusei represents a previously unexplored *Ficus* source of potential EGFR modulators.

Building upon the metabolomic profiling results, the identified metabolites were subjected to target prediction to identify their potential protein targets associated with NSCLC. This analysis identified 362 potential protein targets of Langusei bioactive compounds, which, after integration with disease databases, yielded 355 proteins biologically linked to non-small cell lung cancer (NSCLC). These overlapping targets were subsequently analyzed using network pharmacology to elucidate their functional interactions and prioritize key proteins for downstream ADMET evaluation and molecular docking analyses. Network pharmacology analysis revealed molecular relationships among these targets and key proteins involved in NSCLC pathogenesis, enabling systems-level exploration of the plant's multitarget mechanisms through integrated protein–protein interaction (PPI) data (Zhao et al., 2023).

PPI analysis revealed a highly interconnected network of cancer-related proteins. Topological assessment using four CytoHubba algorithms—Degree, Closeness, Maximum Neighborhood Component (MNC), and Maximal Clique Centrality (MCC)—identified seven hub proteins with the highest centrality values: EGFR, STAT3, EP300, HSP90AA1, JUN, HIF1A, and ESR1. These proteins participate in core oncogenic pathways governing proliferation, angiogenesis, apoptosis resistance, and immune regulation, with EGFR and STAT3 emerging as principal regulatory nodes (Chin et al., 2014; Ashtiani et al., 2018; Li et al., 2019; Christodoulou et al., 2023).

Functional annotation using GO and KEGG confirmed that EGFR and STAT3 play central roles in NSCLC by coordinating cell growth, angiogenesis, apoptosis evasion, immune modulation, and tumor microenvironment remodeling. STAT3 acts as a pleiotropic transcription factor integrating multiple oncogenic cascades, whose persistent activation promotes proliferation, metastasis, metabolic reprogramming, and immune suppression (Zou et al., 2020; Hu et al., 2024). In NSCLC, its inhibition markedly reduces tumor cell survival and reverses immune evasion driven by the IL-6/STAT3 axis (Mohrherr et al., 2020; Parakh et al., 2021; Meraviglia-Crivelli et al., 2022).

Similarly, EGFR functions as both a molecular hub and a primary oncogenic driver initiating and sustaining malignancy in NSCLC. Mutations and overexpression of EGFR underlie a major subset of NSCLC cases, promoting aberrant proliferation, survival, and migration through downstream signaling cascades (Delaney et al., 2015; Halder et al., 2023; La Monica, 2022).

EGFR signaling regulates critical determinants of tumor progression by activating multiple downstream cascades, notably the IL-6/JAK/STAT3 pathway, which induces PD-L1 expression and facilitates immune evasion (Zhang et al., 2016; Hsu et al., 2019). It also contributes to NSCLC tumorigenesis through epigenetic control of the histone demethylase UTX via STAT3 (Zhou et al., 2022). Thus, EGFR acts as an integrative hub coordinating proliferative, survival, and immunoregulatory signaling.

Clinically, EGFR remains a major therapeutic target, driving the development of tyrosine kinase inhibitors (TKIs) as standard therapy for EGFR-mutant NSCLC (Delaney et al., 2015; La Monica, 2022). Third-generation TKIs such as Osimertinib are now first-line treatments, though acquired resistance persists as a major limitation (La Monica, 2022; Fu et

al., 2022). Recent advances—including structure-based EGFR mutation classification and the emergence of allosteric inhibitors that synergize with Osimertinib to overcome ATP-site resistance—highlight continuing progress in overcoming therapeutic resistance (Robichaux et al., 2021; Beyett et al., 2022). Overall, EGFR continues to define the molecular landscape of NSCLC, and elucidating its signaling dynamics is key to improving clinical outcomes (La Monica, 2022).

Drug-likeness screening revealed that all seven bioactive compounds interacted with multiple cancer-related proteins, including EGFR, STAT3, EP300, HSP90AA1, JUN, HIF1A, and ESR1. Among them, only (Z)-1-(1,3-benzodioxol-5-yl)-3-methoxy-3-(2,4,6-trimethoxyphenyl)prop-2-en-1-one showed direct binding to EGFR—the primary oncogenic driver in NSCLC—making it the most promising candidate for EGFR-targeted therapy. Its additional predicted interactions with STAT3, EP300, and JUN suggest a potential multitarget mechanism that could enhance anticancer efficacy.

Among all candidates, the chalcone derivative exhibited the most favorable pharmacokinetic and toxicity profile, with no violations of Lipinski's rules, high intestinal absorption (96%), good Caco-2 permeability, and no predicted hepatotoxicity or cardiotoxicity. It also demonstrated moderate clearance and balanced distribution, indicating good metabolic stability and systemic safety. Membrane permeability simulation further supported these results, showing low free energy of transfer and efficient bilayer penetration. While other compounds displayed auxiliary activity against secondary cancer-related targets, (Z)-1-(1,3-benzodioxol-5-yl)-3-methoxy-3-(2,4,6-trimethoxyphenyl)prop-2-en-1-one stood out as the lead candidate due to its direct EGFR interaction and superior ADMET and drug-likeness profiles, warranting further validation through in vitro and in vivo studies.

Building upon the network and compound identification results, molecular docking was conducted to validate the predicted interactions of the lead compound with the key targets EGFR wild type and its L858R mutant. The docking analysis evaluated the binding affinity and interaction patterns of (Z)-1-(1,3-benzodioxol-5-yl)-3-methoxy-3-(2,4,6-trimethoxyphenyl)prop-2-en-1-one within the EGFR active site, in comparison with the clinical reference ligands Gefitinib and Osimertinib. This approach provided mechanistic confirmation of the compound's pharmacological potential predicted through network and target-based screening.

Docking results demonstrated that the Langusei-derived compound exhibited strong binding affinities toward both EGFR wild type (–6.8 kcal/mol) and the L858R mutant (–6.9 kcal/mol), values comparable to those of the reference inhibitors Gefitinib (–7.9 kcal/mol) and Osimertinib (–7.4 kcal/mol). The small energy differences suggest that the compound can replicate key hydrogen-bonding and hydrophobic interactions within the EGFR active site, supporting complex stability and a comparable inhibitory mechanism. Notably, its slightly higher affinity for the L858R mutant indicates potential selectivity toward this clinically relevant resistant variant. In line with EGFR's functional role, these interactions are closely associated with the ErbB, PI3K–Akt, MAPK, and JAK–STAT signaling pathways, which collectively regulate proliferation, apoptosis resistance, angiogenesis, and immune evasion in NSCLC (Friedlaender et al., 2024).

Together with its favorable ADMET and drug-likeness profile—characterized by high intestinal absorption, optimal solubility, and lack of predicted hepatotoxicity or cardiotoxicity—(Z)-1-(1,3-benzodioxol-5-yl)-3-methoxy-3-(2,4,6-trimethoxyphenyl)prop-2-en-1-one emerges as a novel, naturally derived EGFR inhibitor candidate with promising pharmacological safety. These findings highlight its potential as a lead compound for targeted NSCLC therapy, particularly in overcoming resistance associated with EGFR L858R mutations.

CONCLUSION

This study integrated metabolomic profiling, network pharmacology, and molecular docking to reveal the bioactive potential of Langusei as a natural source of inhibitors targeting the EGFR, particularly the L858R mutant implicated in NSCLC. Combined GC–MS and LC–HRMS analyses identified 170 metabolites dominated by fatty acyls, prenol lipids, and steroid derivatives, reflecting substantial biochemical diversity. Network-based analysis identified seven key proteins, such as EGFR, STAT3, EP300, HSP90AA1, JUN, HIF1A, and ESR1, linked to oncogenic pathways regulating proliferation, angiogenesis, and apoptosis resistance. Among these, EGFR and STAT3 emerged as central regulatory hubs. The compound (Z)-1-(1,3-benzodioxol-5-yl)-3-methoxy-3-(2,4,6-trimethoxyphenyl)prop-2-en-1-one was identified as a novel chalcone-type metabolite with a favorable safety and pharmacokinetic profile. Its predicted interaction with EGFR suggests potential as a natural inhibitor capable of modulating both wild-type and mutant EGFR signaling. Overall, these findings provide a strong foundation for the development of Langusei-derived bioactives as candidate EGFR and STAT3 inhibitors for precision NSCLC therapy. Further in vitro and in vivo validation is essential to confirm their biological efficacy, selectivity, and safety, reinforcing the value of Indonesia's native biodiversity in anticancer drug discovery.

CONFLICT OF INTEREST

The authors declare no conflict of interest related to this study.

ACKNOWLEDGEMENT

This research, conducted under the Master's Thesis Research Scheme for Fiscal Year 2025, was supported by the Directorate of Research and Community Service, Ministry of Higher Education, Science, and Technology of the Republic of Indonesia, under Contract No. 103/C3/DT.05.00/PL/2025, Decree No. 0070/C3/AL.04/2025, and Agreement No. 340/UN12.13/LT/2025.

REFERENCES

Alaaeldin, R., Hassan, H. A., Abdel-Rahman, I. M., Mohyeldin, R. H., Youssef, N., Allam, A. E., Abdelwahab, S. F., Zhao, Q.-L., & Fathy, M. (2022). A New EGFR Inhibitor from *Ficus benghalensis* Exerted Potential Anti-Inflammatory Activity via Akt/PI3K Pathway Inhibition. Current Issues in Molecular Biology, 44(7), 2967-2981. https://doi.org/10.3390/cimb44070205

Alqurashi, Y. E., & Jamal, A. (2024). Targeting epidermal growth factor receptor with Ficus virens metabolites to manage cancer progression: Molecular docking and ADME study. Advances in Human Biology, 14(3), 227–234. https://doi.org/10.4103/aihb.aihb_38_24

Apostol, P. G., De Los Reyes, M. M., Mandia, E. H., Shen, C., & Ragasa, C. Y. (2016). Chemical constituents of Ficus minahassae (Teijsm. & de Vriese) Miq. Der Pharma Chemica, 8(20), 220–223.

Ashtiani, M., Salehzadeh-Yazdi, A., Razaghi-Moghadam, Z., Hennig, H., Wolkenhauer, O., Mirzaie, M., & Jafari, M. (2018). A systematic survey of centrality measures for protein-protein interaction networks. *BMC systems biology*, *12*(1), 80. https://doi.org/10.1186/s12918-018-0598-2

Beyett, T. S., To, C., Heppner, D. E., Rana, J. K., Schmoker, A. M., Jang, J., De Clercq, D. J. H., Gomez, G., Scott, D. A., Gray, N. S., Jänne, P. A., & Eck, M. J. (2022). Molecular basis for cooperative binding and synergy of ATP-site and allosteric EGFR inhibitors. *Nature Communications*, *13*, Article 2530. https://doi.org/10.1038/s41467-022-30258-y

Bray, F., Laversanne, M., Sung, H., Ferlay, J., Siegel, R. L., Soerjomataram, I., & Jemal, A. (2024). Global cancer statistics 2022: GLOBOCAN estimates of incidence and mortality worldwide for 36 cancers in 185 countries. CA: a cancer journal for clinicians, 74(3), 229–263. https://doi.org/10.3322/caac.21834

Cabanlit KL, Torres MAJ, Demayo CG. Ficus spp. (Figs) and their anticancer potential: A systematic review of laboratory studies and traditional uses in the Philippines. J Herbmed Pharmacol. 2025;14(2):133–152.

Cabanlit, K. L., Torres, M. A. J., & Demayo, C. G. (2025). Ficus spp. (Figs) and their anticancer potential: A systematic review of laboratory studies and traditional uses in the Philippines. Journal of Herbmed Pharmacology, 14(2), 133–152. https://doi.org/10.34172/jhp.2025.52854

Cannavacciuolo, C., Pagliari, S., Giustra, C. M., Carabetta, S., Guidi Nissim, W., Russo, M., Branduardi, P., Labra, M., & Campone, L. (2023). LC-MS and GC-MS Data Fusion Metabolomics Profiling Coupled with Multivariate Analysis for the Discrimination of Different Parts of Faustrime Fruit and Evaluation of Their Antioxidant Activity. *Antioxidants*, *12*(3), 565. https://doi.org/10.3390/antiox12030565

Chin, C. H., Chen, S. H., Wu, H. H., Ho, C. W., Ko, M. T., & Lin, C. Y. (2014). cytoHubba: identifying hub objects and sub-networks from complex interactome. *BMC systems biology*, *8 Suppl 4*(Suppl 4), S11. https://doi.org/10.1186/1752-0509-8-S4-S11

Christodoulou, C. C., & Papanicolaou, E. Z. (2023). Integrated Bioinformatics Analysis of Shared Genes, miRNA, Biological Pathways and Their Potential Role as Therapeutic Targets in Huntington's Disease Stages. *International Journal of Molecular Sciences*, *24*(5), 4873. https://doi.org/10.3390/ijms24054873

Delaney, C., Frank, S., & Huang, R. S. (2015). Pharmacogenomics of EGFR-targeted therapies in non-small cell lung cancer: EGFR and beyond. *Chinese Journal of Cancer*, *34*(7). https://doi.org/10.1186/s40880-015-0007-9

Djoumbou Feunang, Y., Eisner, R., Knox, C., Chepelev, L., Hastings, J., Owen, G., Fahy, E., Steinbeck, C., Subramanian, S., Bolton, E., Greiner, R., & Wishart, D. S. (2016). ClassyFire: automated chemical classification with a comprehensive, computable taxonomy. *Journal of cheminformatics*, *8*, 61. https://doi.org/10.1186/s13321-016-0174-y

Friedlaender, A., Perol, M., Banna, G. L., Parikh, K., & Addeo, A. (2024). Oncogenic alterations in advanced NSCLC: A molecular super-highway. *Biomarker Research, 12*(24), 1–30. https://doi.org/10.1186/s40364-024-00566-0

Fu, K., Xie, F., Wang, F., & Fu, L. (2022). Therapeutic strategies for EGFR-mutated non-small cell lung cancer patients with osimertinib resistance. *Journal of Hematology & Oncology*, *15*(173). https://doi.org/10.1186/s13045-022-01391-4

Halder, S., Basu, S., Lal, S., Ganti, A. K., Batra, S. K., & Seshacharyulu, P. (2023). Targeting the EGFR signaling pathway in cancer therapy: What's new in 2023? *Expert Opinion on Therapeutic Targets*, *27*(4-5), 305–324. https://doi.org/10.1080/14728222.2023.2218613

Hu, Y., Dong, Z., & Liu, K. (2024). Unraveling the complexity of STAT3 in cancer: molecular understanding and drug discovery. *Journal of Experimental & Clinical Cancer Research*, *43*(1). https://doi.org/10.1186/s13046-024-02949-5

Hsu, P.-C., Jablons, D. M., Yang, C.-T., & You, L. (2019). Epidermal Growth Factor Receptor (EGFR) Pathway, Yes-Associated Protein (YAP) and the Regulation of Programmed Death-Ligand 1 (PD-L1) in Non-Small Cell Lung Cancer (NSCLC). *International Journal of Molecular Sciences*, *20*(15), 3821.

Sangpheak, K., Tabtimmai, L., Seetaha, S., Rungnim, C., Chavasiri, W., Wolschann, P., Choowongkomon, K., & Rungrotmongkol, T. (2019). Biological Evaluation and Molecular Dynamics Simulation of Chalcone Derivatives as Epidermal Growth Factor-Tyrosine Kinase Inhibitors. *Molecules (Basel, Switzerland)*, *24*(6), 1092. https://doi.org/10.3390/molecules24061092

La Monica, S., Leonetti, A., Tiseo, M., & Alfieri, R. (2022). *EGFR signaling in NSCLC: From molecular understanding to therapeutic innovation. Cells, 11*(8), 1344. https://doi.org/10.3390/cells11081344

Li, C., & Xu, J. (2019). Feature selection with the Fisher score followed by the Maximal Clique Centrality algorithm can accurately identify the hub genes of hepatocellular carcinoma. *Scientific reports*, *9*(1), 17283. https://doi.org/10.1038/s41598-019-53471-0

Lomize, A. L., Hage, J. M., Schnitzer, K., Golobokov, K., LaFaive, M. B., Forsyth, A. C., & Pogozheva, I. D. (2019). PerMM: A Web Tool and Database for Analysis of Passive Membrane Permeability and Translocation Pathways of Bioactive Molecules. *Journal of chemical information and modeling*, *59*(7), 3094–3099. https://doi.org/10.1021/acs.jcim.9b00225

Meraviglia-Crivelli, D., Villanueva, H., Zheleva, A., Villalba-Esparza, M., Moreno, B., Menon, A. P., Calvo, A., Cebollero, J., Barainka, M., Ruiz de los Mozos, I., Huesa-Berral, C., & Pastor, F. (2022). IL-6/STAT3 signaling in tumor cells restricts the expression of frameshift-derived neoantigens by SMG1 induction. *Molecular Cancer*, *21*(1). https://doi.org/10.1186/s12943-022-01679-6

Mohrherr, J., Uras, I. Z., Moll, H. P., & Casanova, E. (2020). STAT3: Versatile Functions in Non-Small Cell Lung Cancer. *Cancers*, *12*(5), 1107. https://doi.org/10.3390/cancers12051107

Pang, H., & Hu, Z. (2023). Metabolomics in drug research and development: The recent advances in technologies and applications. Acta pharmaceutica Sinica. B, 13(8), 3238–3251. https://doi.org/10.1016/j.apsb.2023.05.021

Parakh, S., Ernst, M., & Poh, A. R. (2021). Multicellular Effects of STAT3 in Non-small Cell Lung Cancer: Mechanistic Insights and Therapeutic Opportunities. *Cancers*, *13*(24), 6228. https://doi.org/10.3390/cancers13246228

Pires, D. E., Blundell, T. L., & Ascher, D. B. (2015). pkCSM: Predicting Small-Molecule Pharmacokinetic and Toxicity Properties Using Graph-Based Signatures. *Journal of medicinal chemistry*, *58*(9), 4066–4072. https://doi.org/10.1021/acs.jmedchem.5b00104

Robichaux, J. P., Le, X., Vijayan, R. S. K., Hicks, J. K., Heeke, S., Elamin, Y. Y., Lin, H. Y., Udagawa, H., Skoulidis, F., Tran, H., Varghese, S., He, J., Zhang, F., Nilsson, M. B., Hu, L., Poteete, A., Rinsurongkawong, W., Zhang, X., Ren, C., ... Heymach, J. V. (2021). Structure-based classification predicts drug response in EGFR-mutant NSCLC. *Nature*. https://doi.org/10.1038/s41586-021-03898-1

Salem, M. A., Wang, J. Y., & Al-Babili, S. (2022). Metabolomics of plant root exudates: From sample preparation to data analysis. Frontiers in Plant Science, 13, Article 1062982. https://doi.org/10.3389/fpls.2022.1062982

Parakh, S., Ernst, M., & Poh, A. R. (2021). Multicellular Effects of STAT3 in Non-small Cell Lung Cancer: Mechanistic Insights and Therapeutic Opportunities. *Cancers*, *13*(24), 6228. https://doi.org/10.3390/cancers13246228

Wishart D. S. (2016). Emerging applications of metabolomics in drug discovery and precision medicine. Nature reviews. Drug discovery, 15(7), 473–484. https://doi.org/10.1038/nrd.2016.32

Xie, X., Cai, X., Tang, Y., Jiang, C., Zhou, F., Yang, L., Liu, Z., Wang, L., Zhao, H., Zhao, C., & Huang, X. (2021). Flubendazole Elicits Antitumor Effects by Inhibiting STAT3

and Activating Autophagy in Non-small Cell Lung Cancer. *Frontiers in cell and developmental biology*, *9*, 680600. https://doi.org/10.3389/fcell.2021.680600

Zhang, N., Zeng, Y., Du, W., Zhu, J., Shen, D., Liu, Z., & Huang, J. (2016). The EGFR pathway is involved in the regulation of PD-L1 expression via the IL-6/JAK/STAT3 signaling pathway in EGFR-mutated non-small cell lung cancer. *International Journal of Oncology*, *49*(4), 1360–1368. https://doi.org/10.3892/ijo.2016.3632

Zhao, L., Zhang, H., Li, N., Chen, J., Xu, H., Wang, Y., & Liang, Q. (2023). Network pharmacology, a promising approach to reveal the pharmacology mechanism of Chinese medicine formula. *Journal of ethnopharmacology*, *309*, 116306. https://doi.org/10.1016/j.jep.2023.116306

Zhou, Q., Zhao, H., Lu, S., Cheng, Y., Liu, Y., Zhao, M., Yu, Z., Hu, C., Zhang, L., Yang, F., Zhao, J., Guo, R., Ma, R., Du, Y., Dong, X., Cui, J., Tan, D. S. W., Ahn, M. J., Tsuboi, M., Maggie Liu, S. Y., … Wu, Y. L. (2024). Consensus on the lung cancer management after third-generation EGFR-TKI resistance. The Lancet regional health. Western Pacific, 53, 101260. https://doi.org/10.1016/j.lanwpc.2024.101260

Zhou, L., Wang, X., Lu, J., Fu, X., & Li, Y. (2022). EGFR transcriptionally upregulates UTX via STAT3 in non-small cell lung cancer. *Journal of Cancer Research and Clinical Oncology*, *148*, 309–319. https://doi.org/10.1007/s00432-021-03800-6

Zou, S., Tong, Q., Liu, B., Huang, W., Tian, Y., & Fu, X. (2020). Targeting STAT3 in Cancer Immunotherapy. *Molecular Cancer*, *19*(1). https://doi.org/10.1186/s12943-020-01258-7